Near-infrared spectra of the NaK molecule

J. Huennekens,[a] T. G. Walker, and S. C. McClain

Department of Physics, Princeton University, Princeton, New Jersey 08544

In this paper we present near-infrared absorption, thermal emission, and laser-induced fluorescence spectra obtained in high density sodium–potassium mixtures. These spectra are compared to spectra calculated from recently published NaK potentials and dipole moments and the agreement is seen to be quite good. We have also observed significant laser-induced fluorescence to the red of the $2\ ^1\Sigma^+ \rightarrow 1\ ^1\Sigma^+$ NaK band (A band). From laser power and density dependences of this long-wavelength fluorescence, as well as from comparison to calculated spectra, we have tentatively identified this emission as the lowest NaK triplet band $1\ ^3\Pi \rightarrow 1\ ^3\Sigma^+$ which has not previously been reported. We have also observed a shoulder or satellite feature in potassium vapor under similar conditions. It is possible that this is a potassium trimer emission band.

I. INTRODUCTION

Alkali atoms and molecules have been studied extensively since the last century (see Refs. 1 and 2 for detailed bibliographies of work concerning Li_2 and Na_2). The simple "one electron" nature of the alkalis make them an excellent testing ground of theories of atomic interactions and of calculations of molecular potentials. Alkali atoms and dimers are also attractive from an experimental standpoint since their electronic transitions lie in the visible and near-visible spectral regions. Heteronuclear alkali molecules such as NaK have also been studied extensively for some time, although analysis of their spectra is complicated by overlap from the homonuclear dimer spectra which also much be present.

The visible spectrum of NaK was first systematically studied by Barratt[3] in 1924 and by Walter and Barratt[4] in 1928. The near-infrared $2\ ^1\Sigma^+\text{–}1\ ^1\Sigma^+$ band, commonly referred to as the $A\ ^1\Sigma^+\text{–}X\ ^1\Sigma^+$ or A band (see Fig. 1), was first studied in absorption by Loomis and Arvin.[5] Later, ultraviolet bands were studied by Sinha.[6] More recently, detailed studies of fluorescence following pumping of transitions of the $2\ ^1\Pi \leftarrow 1\ ^1\Sigma^+$ NaK band by Ar^+ laser lines were carried out by Breford and Engelke,[7,8] Eisel, Zevgolis, and Demtroder,[9] and Chiu and Chang.[10] These studies yielded accurate spectroscopic constants for the ground $1\ ^1\Sigma^+$ and the lowest triplet $1\ ^3\Sigma^+$ states. The accuracy of the ground state ($1\ ^1\Sigma^+$) constants were greatly improved by Wormsbecher, Hessel, and Lovas[11] using microwave optical double resonance spectroscopy. Kato and Noda[12] and Kato, Baba, and Hanazaki[13] used Ar^+ laser radiation to study photodissociation processes and intensity distributions in the laser-induced fluorescence (LIF) of the $2\ ^3\Pi \rightarrow 1\ ^3\Sigma^+$ band.

Much recent progress has also been made on calculations of NaK molecular potentials. Roach[14] used a semiempirical valence-electron approximation, while Janoschek and Lee[15] carried out both *ab initio* and pseudopotential calculations. Müller, Flesch, and Meyer[16] and Müller and Meyer[17] have calculated accurate ground state potentials for sev-

eral heteronuclear alkali diatomics including NaK and give an extensive review of the relevant theoretical work. Very recently, full-valence configuration interaction computations of ground and excited state potentials were carried out for NaK by Jeung, Daudey, and Malrieu,[18] Stevens, Konowalow, and Ratcliff,[19] and Bieniek and Olson.[20] These calculated potentials are in good agreement with the available experimental data.

One purpose of the present work was to obtain new data on the near-infrared spectra of NaK. The only detailed study of the NaK $2\ ^1\Sigma^+\text{–}1\ ^1\Sigma^+$ band (A band) is, to the best of our knowledge, that of Loomis and Arvin.[5] They reported a long-wavelength edge of the A band at 1.042 μm but gave details of the absorption band only out to 915 nm. In Sec. III A we present new NaK thermal emission and LIF spectra covering this long wavelength region. These spectra can be used to test the calculated $2\ ^1\Sigma^+$ state potentials.

Alkali vapors are also of interest as laser media. Lasing has been observed on numerous lines of the
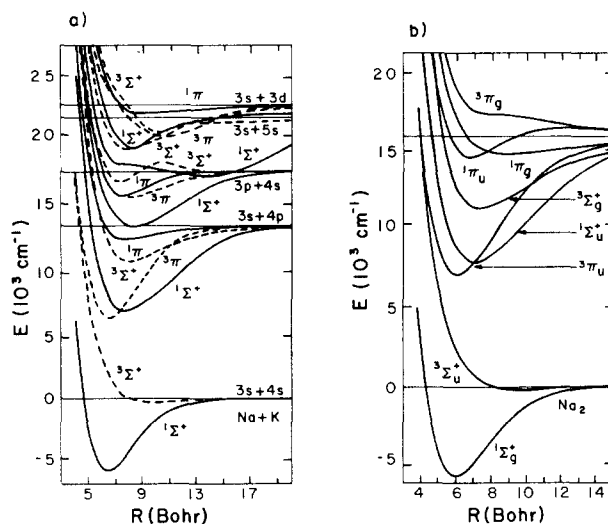
FIG. 1. (a) NaK and (b) Na_2 potential curves taken from Refs. 19 and 29, respectively (figures reproduced with permission from Dr. D. D. Konowalow). Note that throughout the text the notation $2\ ^1\Sigma_g^+$ refers to the second lowest $^1\Sigma_g^+$ state, etc.

[a] Present address: Department of Physics, Lehigh University, Bethlehem, Pennsylvania 18015.

$1\ ^1\Sigma_u^+ \to 1\ ^1\Sigma_g^+$ (A band), $1\ ^1\Pi_u \to 1\ ^1\Sigma_g^+$ (B band), and other singlet bands of Na_2, K_2, and Li_2[21-26] (see Fig. 1). More recently, Kaslin and Yakushev observed lasing on electronic transitions of the heteronuclear molecule NaRb.[27] These alkali dimer lasers operate on a large number of fixed-frequency lines and thus are of practical interest. They also provide much useful information about the alkali molecules themselves. Unfortunately, the discrete nature of the lasing transitions allows only quasi-tunability. Konowalow and Julienne have suggested that continuously tunable near-infrared lasers could be developed utilizing the lowest allowed excimer-like triplet transition $1\ ^3\Sigma_g^+ \to 1\ ^3\Sigma_u^+$ in Li_2 and Na_2.[28] Until recently, these low lying triplet transitions escaped detection due to the difficulty of populating the upper triplet states, the awkward emission wavelengths from the standpoint of detectors, and the overlapping of these bands by the stronger $1\ ^1\Sigma_u^+ \to 1\ ^1\Sigma_g^+$ band. In work guided by the accurate potential calculations of Konowalow and co-workers,[29-31] these $1\ ^3\Sigma_g^+ \to 1\ ^3\Sigma_u^+$ bands have been observed and identified in Na_2 and K_2.[32-35] The possibility of achieving lasing on these transitions is being pursued in this laboratory. However, as can be seen from the spectra of Ref. 35, much of the broadband tunability promised by these lasers would be lost to self-absorption in the $1\ ^1\Sigma_u^+ - 1\ ^1\Sigma_g^+$ bands.

The self-absorption problem might be avoided in heteronuclear alkali molecules such as NaK. In these molecules the g, u symmetries of the wave functions under inversion of electron coordinates through a center of symmetry do not exist. Consequently, the lowest allowed triplet transition is the $1\ ^3\Pi \to 1\ ^3\Sigma^+$ band (see Fig. 1), which is the analog of the forbidden $1\ ^3\Pi_u \to 1\ ^3\Sigma_u^+$ band in the homonuclear molecules. In Sec. III B we report the observation of infrared fluorescence at wavelengths longer than the NaK $2\ ^1\Sigma^+ - 1\ ^1\Sigma^+$ (A-X) band satellite in high density sodium–potassium vapors excited by Kr^+ laser radiation. By studying the infrared emission intensity as a function of incident laser power and relative Na and K densities, as well as by comparison with calculated fluorescence spectra, we tentatively identify this emission as the $1\ ^3\Pi \to 1\ ^3\Sigma^+$ transition of NaK. We also present data in Sec. III B of an LIF satellite feature observed in potassium vapor at $\sim 1.29\mu m$ which may be a triatomic (K_3) emission feature.

Finally, in Sec. III C we report a complete visible and near-infrared absorption spectrum of a high-density (~ 150 Torr) sodium–potassium mixture. Such a spectrum, consisting of strong Na_2, K_2, and NaK absorption bands which almost completely cover the visible and near-IR regions, is of interest since mixed alkali vapors are under consideration as the working medium in efficient solar absorbers.[36-37]

Our results are summarized and discussed in Sec. IV.

II. THE EXPERIMENT

The high-density alkali jet device used to obtain the spectra presented here has been described in Refs. 33–35. Thus we will only give a brief account of it in this paper. This device is a flowing gas system in which alkali metal vapor is contained by a flowing sheath of argon gas. The alkali boils in a stainless steel can and the vapor flows up and out a

vertical chimney. Argon gas flows upward in a concentric ring surrounding the chimney, so where the metal vapor emerges from the chimney it is confined by the flowing argon sheath. By an approximate match of argon and alkali flow velocities, laminar flow is established for a couple of centimeters above the chimney, creating a well-defined column of dense alkali vapor ($\sim 10^{18}$ atoms/cm^3 or pressures in the 70–250 Torr range). This region is accessed by four arms supporting cooled Pyrex windows which are set back ~ 13 cm from the hot vapor. After passing the viewing region, the alkali enters a cooler section where the metal condenses. It then falls back to the boiler under the influence of gravity. The argon gas is siphoned off and recirculated through its own closed loop. As described in Ref. 35, we used a standard optical setup (see Fig. 2 of Ref. 35) to obtain absorption, thermal emission, and laser-induced fluorescence (LIF) spectra. In the present experiment, photons from the alkali vapor region were dispersed by a 0.3 m monochromator and detected with either a photomultiplier (RCA 7102 or EMI 9558 with S-1 and S-20 cathode responses, respectively) or an intrinsic germanium detector (North Coast EO-917L). In all cases we mechanically chopped either the laser, the lamp used for absorption, or the thermal emission itself, and employed lock-in techniques. Relative detection system efficiencies were obtained using a calibrated blackbody source. For LIF spectra we primarily used the 1–5 W output of a multimode Kr^+ laser operating on the red lines 647.1 and 676.4 nm (an RG 610 long-pass filter was used to block any laser emissions with $\lambda < 610$ nm). Occasionally we instead used the ~ 300 mW multimode output of an Oxazine dye laser or 1–3 W from a multimode argon ion laser operating on one of the blue or green lines. These high powers were necessary to penetrate the large optical depth of the vapor column. Relative densities of sodium and potassium atoms were varied simply by changing the composition of the bulk metal loaded into the boiler prior to the run. As a warning to anyone interested in building such a device based on the designs of Ref. 33, we note that the highly corrosive alkalis take their toll even on the 304L stainless steel. Near the end of this experiment two welds gave way revealing extensive corrosion. Fortunately, these weld failures occurred during cleaning rather than during operation at high temperature where they may have presented a serious physical danger. Nevertheless, the device operated in a fairly reliable fashion for more than two years before the corrosion reached this level.

III. RESULTS

A. NaK $2\ ^1\Sigma^+ \to 1\ ^1\Sigma^+$ band thermal emission and laser-induced fluorescence

Figure 2 shows a thermal emission spectrum obtained from the high-density jet device at a temperature of ~ 710 °C. For this data, we loaded the boiler with an approximately 90% sodium -10% potassium mixture to reduce the $K_2\ 1\ ^1\Sigma_u^+ \to 1\ ^1\Sigma_g^+$ and $1\ ^3\Sigma_g^+ \to 1\ ^3\Sigma_u^+$ band emissions (see Fig. 1) which overlap the NaK $2\ ^1\Sigma^+ \to 1\ ^1\Sigma^+$ band. This proved effective, as these known K_2 bands appeared with negligible intensity in our spectrum. The significant emission to the red of the NaK A band satellite follows a
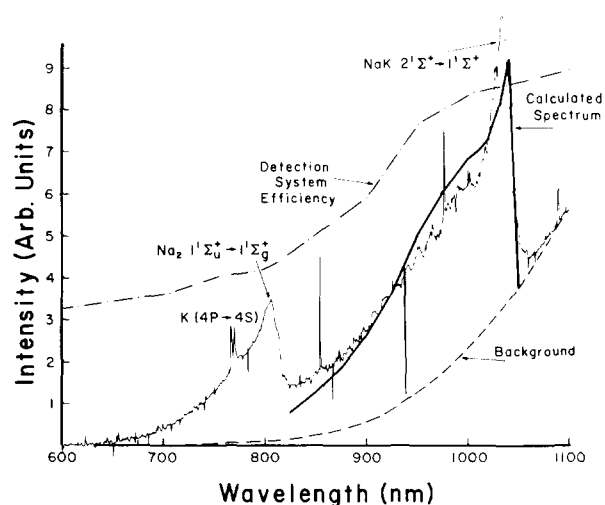
FIG. 2. Thermal spectrum (thin solid line) obtained using the intrinsic Ge detector and the high-density jet apparatus with an ~90% sodium–10% potassium mixture. The temperature was ~711 °C, total pressure was ~155 Torr, and spectral resolution ~1.1 nm. The dashed line represents the background signal (corrected for detection system efficiency) due to scatter of blackbody wall emission by small droplets in the jet. The thick solid line is the NaK thermal spectrum (normalized to the experimental spectrum at 1.02 μm and adjusted for detection system efficiency to aid comparison with the data) calculated from the potentials and dipole moments of Ref. 19 and Eqs. (1)–(4). The dot–dash line at the top is the relative detection system efficiency measured using a calibrated blackbody source.

blackbody curve, convoluted with our detector efficiency, as far as we can follow it to the long-wavelength edge of the Ge detector response. We believe this is simple scatter of blackbody wall radiation by small droplets in the jet.[35] Similar emission, but of lower overall intensity, was observed when we studied pure alkalis.[35] The droplet problem is more severe in the alkali mixture since inhomogeneities in the mixture cause the boiling to be more erratic. For our purposes, the background blackbody emission due to this scatter can be removed by a simple baseline correction. Since the density of Na_2 molecules was roughly an order of magnitude larger than that of NaK, we also observed significant Na_2 $1\,^1\Sigma_u^+ \rightarrow 1\,^1\Sigma_g^+$ band thermal emission.

As a comparison with theory, we used the most recent NaK potentials and dipole moments available[19] to calculate an NaK $2\,^1\Sigma^+ \rightarrow 1\,^1\Sigma^+$ band thermal emission spectrum. To do this we first calculated the frequency dependent absorption coefficient using quasistatic line broadening theory,[38–41] i.e.,

$$k_v(T) = \frac{8\pi^4 vD^2 g^*}{3hc}\, n_{Na} n_K \frac{[R(v)]^2}{|dv/dR|} e^{-V/kT},\qquad (1)$$

where $R(v)$ is the internuclear separation that yields a difference potential hv, D is the transition dipole moment at R, V is the ground state potential at R, g^* is the upper state statistical weight (1 for the $2\,^1\Sigma^+ \rightarrow 1\,^1\Sigma^+$ band), and n_{Na} and n_K are the sodium and potassium atom densities, respectively. [This equation is the same as Eq. (1), Ref. 35 with $n^2/2$ replaced by $n_{Na} n_K$. The factor of 2 in the earlier expression resulted from the fact that the interacting atoms are identical in that case. Note also that the factor $3hc$ was inadvertantly left out of Eq. (1), Ref. 35.] The derivative dv/dR was calculated using a simple three point average which sidesteps the

problem of creating a nonphysical singularity at the satellite point. The thermal emission $I(v,T)$ is related to the absorption coefficient by Kirchhoff's Law:

$$I(v,T) = \epsilon_v I_{BB}(v,T),\qquad (2)$$

where $I_{BB}(v,T)$ is the emission spectrum of a perfect blackbody at temperature T, given by the Planck formula

$$I_{BB}(v,T) = \frac{8\pi hv^5}{c^4}\,[e^{hv/kT} - 1]^{-1},\qquad (3)$$

and the emissivity ϵ_v equals the absorptivity α_v defined for a path length L by the expression

$$\epsilon_v = \alpha_v = 1 - e^{-k_v L}.\qquad (4)$$

The calculated thermal spectrum was adjusted for detection system efficiency to aid comparison with the data, then normalized to the experimental signal (minus the background due to scatter by droplets) at 1.02 μm, added to the background, and plotted in Fig. 2. The detailed shape of the calculated satellite peak cannot be expected to match the experimental curve since the former was obtained using the classical quasistatic theory which is known to break down in the satellite region. The satellite position should be given reasonably well by the calculation, however. It has been shown[42] that the satellite wavelength predicted from the quasistatic calculation (corresponding to the extremum of the difference potential) matches the wavelength of the 65% intensity point on the far side of the more realistic semiclassical Sando–Wormhoudt[43] satellite. The simple quasi-static calculation, using the Steven's et al.[19] potentials, predicts a 65% intensity point at $\lambda = 1.043$ μm in excellent agreement with the observed value 1.040 μm. The observed satellite peak intensity occurs at 1.033 μm. {This separation of ~70 Å between satellite peak and 65% intensity point is in good agreement with the value 63 Å predicted by the Sando–Wormhoudt theory[43] [i.e., see Eq. (5) in Sec. III B] using the second derivative of the difference potential obtained from the potentials of Ref. 19.} Thus the Steven's et al.[19] potentials predict the satellite wavelength to within 0.3%. The analogous errors of ~2.1% and ~2.8% for the Na_2 and K_2 $1\,^1\Sigma_u^+ \rightarrow 1\,^1\Sigma_g^+$ band satellite positions calculated from the potentials and dipole moments of Refs. 29–31 were determined using the 65% rule and the data of Ref. 35.

Figure 3 shows an LIF spectrum obtained in the jet apparatus under conditions similar to those of Fig. 2. The excitation source for this spectrum was the Kr^+ laser operating at 647.1 and 676.4 nm with 3 W total power. These laser lines primarily pump the Na_2 $1\,^1\Sigma_u^+ -1\,^1\Sigma_g^+$ band for our vapor composition, but they also pump the NaK $1\,^1\Pi-1\,^1\Sigma^+$ and $3\,^1\Sigma^+ -1\,^1\Sigma^+$ and the K_2 $1\,^1\Pi_u -1\,^1\Sigma_g^+$ (B–X) bands (see Fig. 1) to a lesser degree. Thus the directly pumped Na_2 $1\,^1\Sigma_u^+ \rightarrow 1\,^1\Sigma_g^+$ band displays some vibrational structure characteristic of LIF while most of the structure of the emission from the collisionally populated NaK $2\,^1\Sigma^+$ state is washed out.

Under the same excitation conditions, LIF spectra in the visible revealed overlapping K_2 and NaK $1\,^1\Pi \rightarrow 1\,^1\Sigma^+$ bands (which are directly excited by the laser) and the collisionally produced Na_2 $1\,^1\Pi \rightarrow 1\,^1\Sigma^+$ fluorescence. Since the LIF emission must pass through ~1/2 cm of unexcited
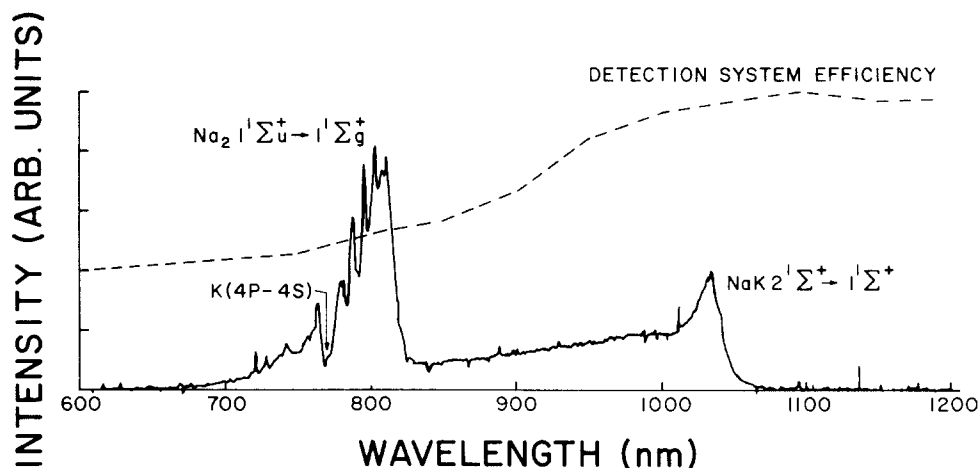
FIG. 3. Laser-induced fluorescence from the $\sim 90\%$ sodium–10% potassium mixture in the high-density jet apparatus. The vapor temperature was ~ 711 °C and the total pressure ~ 157 Torr. Excitation was by $\sim 3W$ of Kr^+ laser power at 647.1 and 676.4 nm. Spectral resolution was ~ 2.7 nm. The spectrum was obtained using the intrinsic Ge detector. A 610 nm long pass filter was placed in front of the monochromator to block second order spectra. Since the laser-induced fluorescence must pass through $\sim 1/2$ cm of unexcited vapor before reaching the detector much self-absorption occurs. In particular, almost all emission between 600 and 700 nm is self-absorbed. This effect also explains why the potassium resonance lines appear here in absorption whereas they occur in emission in the thermal scan (Fig. 2).

vapor much self-absorption occurs (see also Fig. 9). Fluorescence from higher lying states was not observed in our experiment although we did not extensively pursue this point since our main interest was the infrared bands.

B. Long wavelength LIF

In diatomic molecules composed of atoms of unequal nuclear charge there is no symmetry under inversion of electron coordinates through a point. Consequently, in NaK, we expect to be able to observe $1\ ^3\Pi \to 1\ ^3\Sigma^+$ band fluorescence which is the analog of the forbidden $1\ ^3\Pi_u \to 1\ ^3\Sigma_u^+$ band in homonuclear alkali molecules (see Fig. 1). In NaK the dissimilarity between the nuclear charges is not so great as to make this band as strong as fully allowed transitions, and Stevens et al.[19] have calculated dipole moments for the NaK $1\ ^3\Pi \to 1\ ^3\Sigma^+$ band which are roughly a factor of 5 smaller than those of the $2\ ^1\Sigma^+ \to 1\ ^1\Sigma^+$ band. Additionally, direct pumping of the $1\ ^3\Pi$ state from the ground state $1\ ^1\Sigma^+$ is inefficient due to the $\Delta S = 0$ dipole selection rule. (Note that this selection rule is less strictly enforced in heavier molecules. Nevertheless, Li and Field and Li, Rice, and Field have recently carried out a series of optical–optical double resonance experiments in Na_2 where $1\ ^3\Pi_u \gets 1\ ^1\Sigma_g^+$ transitions were pumped in the first step.[44–45]) However, the $1\ ^3\Pi$ state is the lowest state of the first excited manifold in all the alkali dimers and collisional mechanisms tend to filter population down to it. We therefore expect that laser pumping of higher states in the first excited manifold will result in $1\ ^3\Pi \to 1\ ^3\Sigma^+$ fluorescence lying to the red of the $2\ ^1\Sigma^+ \to 1\ ^1\Sigma^+$ band.

We have searched for this emission from high density sodium–potassium mixtures in the jet apparatus following excitation with the Kr^+ laser lines 647.1 and 676.4 nm. Figure 4 shows the fluorescence spectrum to the red of the NaK $2\ ^1\Sigma^+ \to 1\ ^1\Sigma^+$ band satellite for an approximately 50–50 mixture of sodium and potassium and a total pressure of

~ 157 Torr. Molecular fluorescence which monotonically decreases with increasing wavelength was observed in the region 1.1–1.7 μm. We verified, using filters and independent tests of the monochromator, that the long wavelength
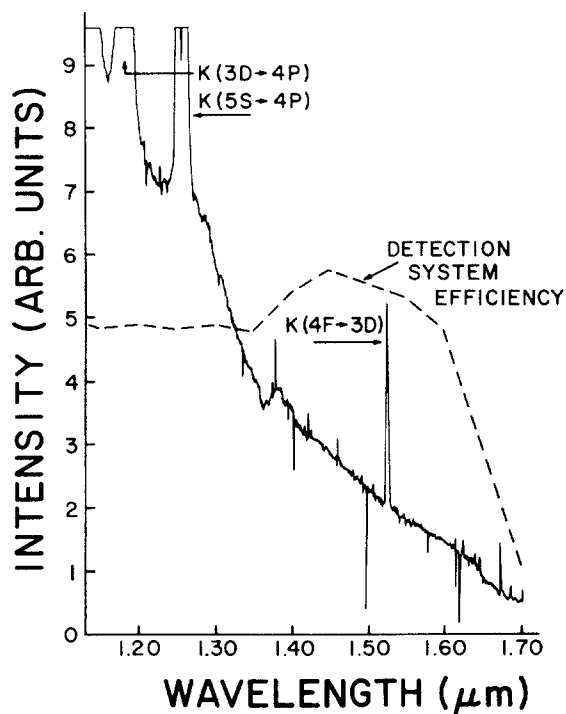
FIG. 4. Long wavelength laser-induced molecular fluorescence obtained in an ~ 50–50 mixture of sodium and potassium in the high-density jet apparatus. Total alkali pressure was ~ 157 Torr and the temperature ~ 721 °C. The spectrum was obtained with the intrinsic Ge detector and an ~ 3.2 nm resolution. Excitation was by the Kr^+ laser lines 647.1 and 676.4 nm with a total power of $\sim 5W$. Sharp spikes in the spectrum, other than the labeled atomic lines are due to cosmic rays to which the Ge detector is sensitive. The dashed line represents the relative detection system efficiency.
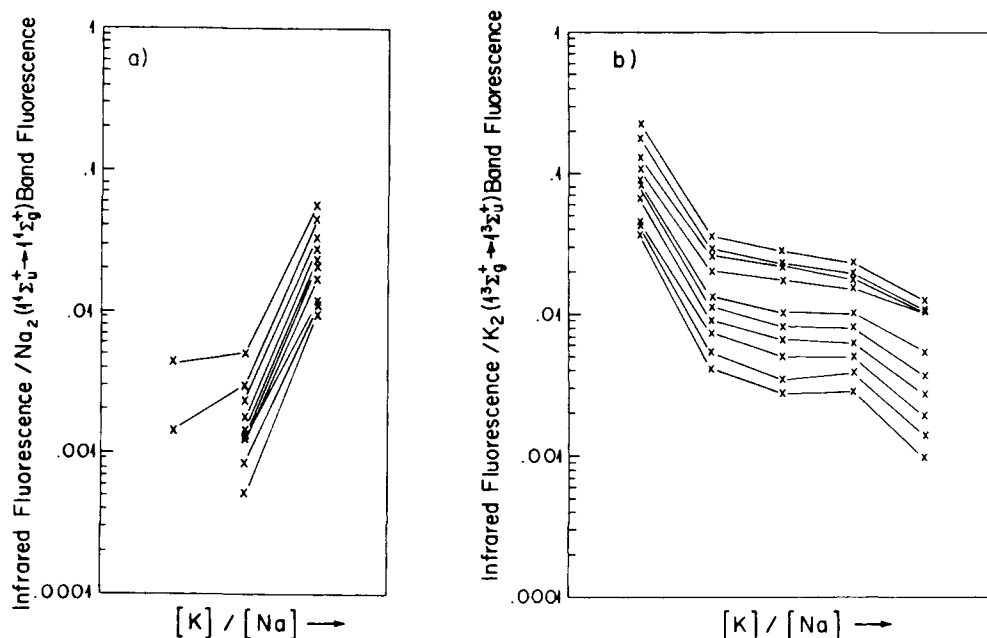
FIG. 5. Plot of long-wavelength fluorescence intensity normalized to (a) the Na_2 $1\ ^1\Sigma_u^+ \rightarrow 1\ ^1\Sigma_g^+$ and (b) the K_2 $1\ ^3\Sigma_g^+ \rightarrow 1\ ^3\Sigma_u^+$ fluorescence intensity (this potassium triplet band is described in more detail in Ref. 35) vs the ratio of potassium to sodium density ([K]/[Na]) with total pressure fixed at a constant value of ~ 156 Torr. Note that the abscissa is a nonlinear scale as [K]/[Na] was varied systematically but not monitored for each point. Thus only the ordering of the points is significant. From top to bottom the curves represent emission at 1.20, 1.25, 1.30, 1.35, 1.40, 1.45, 1.50, 1.55, and 1.60 μm but no corrections were made for detection system efficiency. The leftmost set of points in part (a) correspond to pure Na ($\sim 0.01\%$ K) while the rightmost set of points in part (b) correspond to pure K ($\sim 98\%$ K, $\sim 2\%$ Na). The rightmost set of points in part (a) and the leftmost in part (b) correspond to the same data (but with different normalization).

fluorescence was not simple leakage of $2\ ^1\Sigma^+ \rightarrow 1\ ^1\Sigma^+$ band fluorescence through the monochromator. Fluorescence from potassium atomic transitions ($3D \rightarrow 4P$, $5S \rightarrow 4P$, and $4F \rightarrow 3D$) can also be seen in Fig. 4.

Classically no $2\ ^1\Sigma^+ \rightarrow 1\ ^1\Sigma^+$ (A band) fluorescence is expected at wavelengths longer than the satellite wavelength. Semiclassically or quantum mechanically we expect an exponential fall off past the satellite, and since the long wavelength fluorescence reported in Fig. 4 does look like an exponential tail on the red side of the $2\ ^1\Sigma^+ \rightarrow 1\ ^1\Sigma^+$ band, we must consider this possibility. According to Sando and Wormhoudt's semiclassical theory[43] the fall off on the dark side of the satellite obeys

$$I(v) \propto u^{-1/2} \exp(-2.29u), \qquad (5)$$

where $u \simeq [\mu/(\hbar^2 kT\Delta V'')]^{1/3} h (v_s - v)$, μ is the reduced mass of the Na–K collision system, $v_s = c/\lambda_s$ is the position of the satellite, and $\Delta V''$ is the second derivative of the difference potential with respect to internuclear separation. Equation (5) has been verified qualitatively in experiment[42] as well as in comparison to quantum mechanical calculations.[43] For our system, using the potentials of Steven's et al.,[19] Eq. (5) predicts that the satellite intensity should fall off more than six orders of magnitude by $\lambda = 1.20\ \mu$m. Experimentally, the signal at $1.20\ \mu$m is 0.007 times the peak intensity. Thus this long wavelength emission is not just the tail of the $2\ ^1\Sigma^+ \rightarrow 1\ ^1\Sigma^+$ band fluorescence.

Three pieces of evidence lead us to conclude that this long wavelength molecular fluorescence is at least in part composed of NaK $1\ ^3\Pi \rightarrow 1\ ^3\Sigma^+$ emission. First, we have studied the emission intensity as a function of vapor composition. The results of that study are presented in Fig. 5 where we plot long wavelength molecular fluorescence intensity (normalized to either the K_2 $1\ ^3\Sigma_g^+ \rightarrow 1\ ^3\Sigma_u^+$ or Na_2 $1\ ^1\Sigma_u^+ \rightarrow 1\ ^1\Sigma_g^+$ band peak intensities) vs the ratio of potassium to sodium density ([K]/[Na]) with the total pressure

fixed at ~ 150 Torr. Note that the x axis is nonlinear as we did not have a direct measure of the relative vapor composition through most of the data acquisition process. Nevertheless, the points are ordered correctly along the x axis, since we were able to vary [K]/[Na] systematically by simply changing the composition of the alkali mixture in the boiler while maintaining a constant total pressure. In each run of the jet, some metal is lost from the alkali circulation loop to the argon circulation system filters (see Refs. 33–35), and the device must therefore be partially reloaded before a second run. For out first run we used an approximately 50–50 mixture of Na and K. For the second and subsequent runs we loaded pure potassium to the mixture already present, so that in each case the [K]/[Na] ratio was increased relative to the previous run. This data corresponds to that shown in Fig. 5(b). For the data in Fig. 5(a), the same procedure was used but the initial "mixture" in this case was pure Na.

We expect that NaK fluorescence will scale as the product [Na][K] (with the total pressure remaining constant) while Na_2 and K_2 fluorescence will scale as $[Na]^2$ and $[K]^2$, respectively. Thus if we normalize to the intensity of a known K_2 band ($1\ ^3\Sigma_g^+ \rightarrow 1\ ^3\Sigma_u^+$) we expect NaK fluorescence will scale as $([K]/[Na])^{-1}$, Na_2 fluorescence will scale as $([K]/[Na])^{-2}$, and K_2 fluorescence as a constant. Similarly if we normalize to a known Na_2 band ($1\ ^1\Sigma_u^+ \rightarrow 1\ ^1\Sigma_g^+$) intensity, we expect NaK fluorescence will scale as [K]/[Na], K_2 fluorescence as $([K]/[Na])^2$, and Na_2 fluorescence as a constant. The data of Fig. 5 are clearly consistent with the long wavelength fluorescence originating from the NaK molecule. Normalization to other observed NaK bands was impossible due to overlap with Na_2 and K_2 bands. Note that the large quantities of alkalis necessary to run the jet device precluded using high purity Na and K. Thus our "pure" K metal contains $\sim 2\%$ Na while the "pure" Na contains $\sim 0.01\%$ K.

The data presented in Fig. 5 are not conclusive since the

normalization procedure itself may depend on the relative Na and K densities. The Kr^+ laser directly pumps the Na_2 $1\,^1\Sigma_u^+ \leftarrow 1\,^1\Sigma_g^+$, $K_2\,1\,^1\Pi_u \leftarrow 1\,^1\Sigma_g^+$, NaK $3\,^1\Sigma^+ \leftarrow 1\,^1\Sigma^+$, and NaK $1\,^1\Pi \leftarrow 1\,^1\Sigma^+$ (and to a lesser extent K_2 $1\,^1\Sigma_u^+ \leftarrow 1\,^1\Sigma_g^+$ and NaK $2\,^1\Sigma^+ \leftarrow 1\,^1\Sigma^+$) transitions with relative populations depending on vapor composition. Since the K_2 $(1\,^3\Sigma_g^+)$ state and the upper state of the long-wavelength fluorescence are populated by various and different collisional processes, it is clear that their relative population rates may depend on vapor composition. It is not unreasonable to expect that this dependence would be proportional to $([K]/[Na])^{-1}$ as indicated above, but it is also possible that the actual situation is more complicated. We can therefore only say that the data of Fig. 5 are strongly suggestive of an NaK origin of the long-wavelength molecular fluorescence.

The second piece of evidence supporting our interpretation of the long wavelength fluorescence as due in part to NaK $1\,^3\Pi \rightarrow 1\,^3\Sigma^+$ is the dependence of the fluorescence intensity on laser power. If states above the first excited manifold were involved in the observed fluorescence, we would expect at least a quadratic dependence of fluorescence intensity on laser power, unless one or the other excitation step was saturated. For the very high densities and cw laser powers used here, the situation is complicated by the nonlinear manner in which the laser burns through the vapor (e.g., local heating of the vapor by the laser may reduce the local molecular concentration through dissociation). We found significant variability in the slopes of log–log plots of long wavelength fluorescence vs laser power for different vapor compositions but the average value obtained was 1.1. We rule out saturation since the potassium $3D$, $5S$, and $4F$ atomic line intensities vary roughly cubically with laser power (implying the atomic emission probably results from ionization followed by recombination). Since the laser is not resonant with either one-photon or two-photon atomic transitions, we can trace these atomic excitations back to the same molecular absorption as lead to the long-wavelength fluorescence. The atomic fluorescence laser power dependence indicates that these molecular transitions are not saturated. Simple calculations also indicate that saturation is not occuring at these high molecular densities. The laser power dependence, like the density dependence, is also not conclusive, but is suggestive that the observed fluorescence stems from the first excited manifold of the NaK molecule.

The final identification of the long wavelength fluorescence rests on comparison of the observed spectrum with spectra calculated from the NaK potentials and dipole moments of Ref. 19. Laser-induced fluorescence spectra were calculated from the quasistatic theory expression

$$I(v) \propto g^* \left(\frac{v}{v_0}\right)^4 \frac{R^2(v)}{|dv/dR|}\,D^2 e^{-V^*/kT_{eff}} \tag{6}$$

(see Ref. 35), where V^* is the upper state potential at R and T_{eff} is the effective excitation temperature (which was taken to be 3700 K). Spectra were calculated for all possible near-infrared bands (including those forbidden by the $\Delta S = 0$ selection rule) originating in the first excited manifold of NaK. As can be seen in Fig. 6, where the most important of these
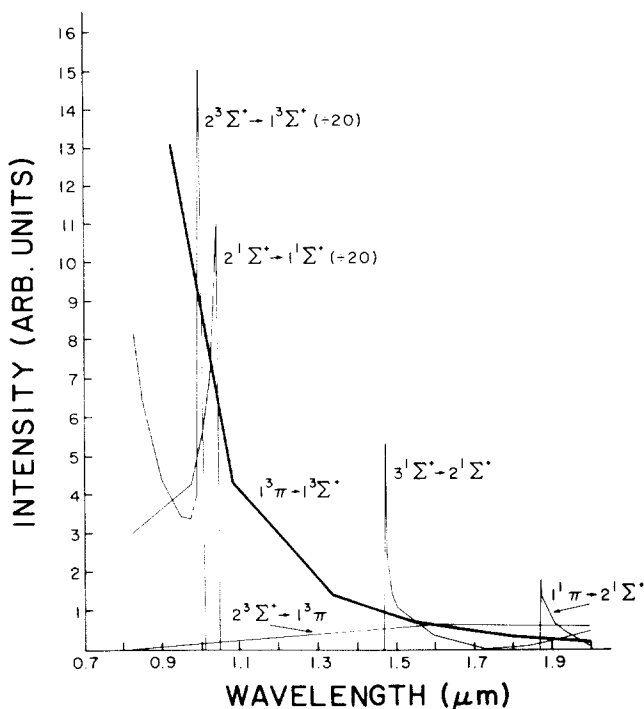
FIG. 6. Calculated LIF spectra of various NaK bands with upper states in the first excited manifold. Calculations are based upon Eq. (6) and the potentials and dipole moments of Ref. 19 using an effective excitation temperature of 3700 K. The $1\,^3\Pi \rightarrow 1\,^3\Sigma^+$ band is depicted by the thick solid line.

calculated bands are plotted, only the $1\,^3\Pi \rightarrow 1\,^3\Sigma^+$ transition is predicted to radiate over the full wavelength range where long-wavelength fluorescence was observed. Additionally the observed monotonic decrease in intensity with increasing wavelength is also predicted by the calculations. In fact the predicted and observed wavelength dependencies are in very good agreement. We note that for the $1\,^3\Pi \rightarrow 1\,^3\Sigma^+$ band the quasistatic theory calculations [Eq. (6)] should yield accurate results since there are no extrema in the difference potential. The choice of 3700 K as the effective excitation temperature (which is simply the value that gave a good match between experiment and calculation in a similar LIF experiment in Na_2^{35}) is rather arbitrary. We therefore demonstrate in Fig. 7 that the shape of the calculated $1\,^3\Pi \rightarrow 1\,^3\Sigma^+$ spectrum is fairly independent of the excitation temperature chosen. Finally we note that the predicted relative magnitudes of $1\,^3\Pi \rightarrow 1\,^3\Sigma^+$ and $2\,^1\Sigma^+ \rightarrow 1\,^1\Sigma^+$ band emissions agree to within approximately a factor of 2 which is extremely good considering self-absorption of the $2\,^1\Sigma^+ \rightarrow 1\,^1\Sigma^+$ band and the other large uncertainties. For completeness we calculated LIF spectra for Na_2 and K_2 bands originating in the first excited manifold (using potentials and dipole moments of Refs. 29–31) but found nothing consistent with the long-wavelength fluorescence.

Note that the mutual perturbation of the $1\,^3\Pi$ and $2\,^1\Sigma^+$ states near their crossing point at $R \sim 7.4$ a.u.[19] (see Fig. 1) results in wave functions which are linear combinations of the two states. This greatly complicates the calculation of both the $2\,^1\Sigma^+ \rightarrow 1\,^1\Sigma^+$ and $1\,^3\Pi \rightarrow 1\,^3\Sigma^+$ spectra
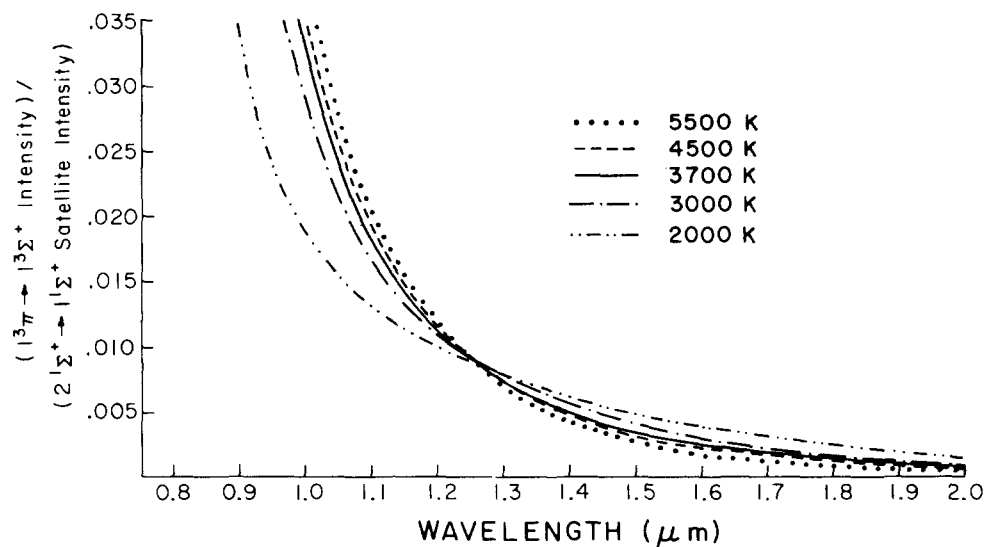
FIG. 7. Calculated LIF spectra of the NaK $1\,^3\Pi \to 1\,^3\Sigma^+$ band (normalized to the calculated NaK $2\,^1\Sigma^+ \to 1\,^1\Sigma^+$ band satellite intensity) for several values of the effective excitation temperature used in Eq. (6). As in Figs. 2 and 6 these calculations employ the potentials and dipole moments of Ref. 19. Note that the normalized $1\,^3\Pi \to 1\,^3\Sigma^+$ band intensity is independent of excitation temperature near 1.26 μm. (This is due to the fact that the $1\,^3\Pi$ potential energy at the internuclear separation where 1.26 μm photons originate is equal to the $2\,^1\Sigma^+$ potential energy at the internuclear separation where $2\,^1\Sigma^+ \to 1\,^1\Sigma^+$ satellite photons originate.) At 1.26 μm the observed normalized intensity is ~0.0062 which is within 35% of the calculated value.

since the $2\,^1\Sigma^+ \to 1\,^3\Sigma^+$ and $1\,^3\Pi \to 1\,^1\Sigma^+$ contributions must be considered as well as interference terms. However, the effect of this mixing on the $2\,^1\Sigma^+ \to 1\,^1\Sigma^+$ satellite region (i.e., as shown in Fig. 2) is not severe because the satellite fluorescence is associated with internuclear separations near $R = 10$ a.u. According to the potentials of Ref. 19, the $1\,^3\Pi \to 1\,^1\Sigma^+$ contribution to the $2\,^1\Sigma^+ \to 1\,^1\Sigma^+$ band should be insignificant for wavelengths longer than 900 nm. This effect may, however, contribute to the underestimation of our calculated $2\,^1\Sigma^+ \to 1\,^1\Sigma^+$ emission between 800 and 900 nm relative to the emission at slightly longer wavelengths. The contribution of $2\,^1\Sigma^+ \to 1\,^3\Sigma^+$ to the calculated $1\,^3\Pi \to 1\,^3\Sigma^+$ emission spectra shown in Fig. 6 is expected to be most significant in the 1.3–1.5 μm region, according to the potentials.[19] Clearly our experiment does not distinguish these two types of emission but measures only total fluorescence in that wavelength region. However, the calculations of Fig. 6 are meant only to give a rough idea of the locations and shapes of the various bands, not to yield high precision spectra.

Note also that the calculated $1\,^3\Pi$ and $1\,^3\Sigma^+$ states[19] (see Fig. 1) converge and cross on their repulsive limbs. This could lead to predissociation of the $1\,^3\Pi$ state as it thought to occur for the analogous states of Li_2.[30,46] For NaK, however, the Stevens et al. potentials[19] indicate that this crossing occurs high up on the repulsive wall, so we expect no significant predissociation in this case. Our experimental data shed little light on this question except that the observed relative intensities of the $1\,^3\Pi \to 1\,^3\Sigma^+$ and $2\,^1\Sigma^+ \to 1\,^1\Sigma^+$ bands are inconsistent with strong predissociation of the $1\,^3\Pi$ state.

We believe that the data presented above make a strong case that the long wavelength fluorescence seen in Fig. 4 is in fact the NaK $1\,^3\Pi \to 1\,^3\Sigma^+$ band. Implications of this identification for the development of tunable alkali near infrared lasers are discussed in Sec. IV.

We also note that the wavelength dependence of the long-wavelength fluorescence changed as the vapor composition approached "pure" potassium. In particular a shoulder or satellite feature appeared in the spectrum with a peak near 1.29 μm. This is shown in Fig. 8. The shoulder was

found to scale linearly with laser power. An attempt was made to study the dependence of this 1.29 μm emission on potassium density, but the results were inconclusive. It is possible that this shoulder feature seen here in emission may correspond to a bump near 1.26 μm in the absorption spectrum of high density potassium vapor.[47–49] This weak absorption, which was observed in Refs. 47–49, was attri-
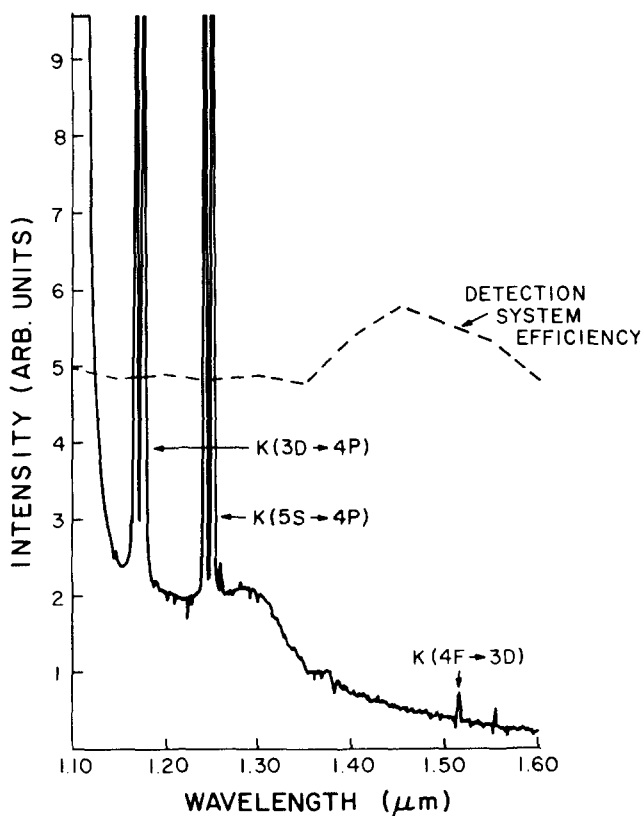
FIG. 8. Near-infrared LIF spectrum obtained from an ~156 Torr pure potassium vapor excited by the 647.1 and 676.4 nm Kr^+ laser lines. $T = 706$ °C. The spectrum was obtained with the intrinsic Ge detector at a resolution of 1.6 nm. Dashed line represents the detection system efficiency. The shoulder feature peaking at ~1.29 μm may be a K_3 emission band.
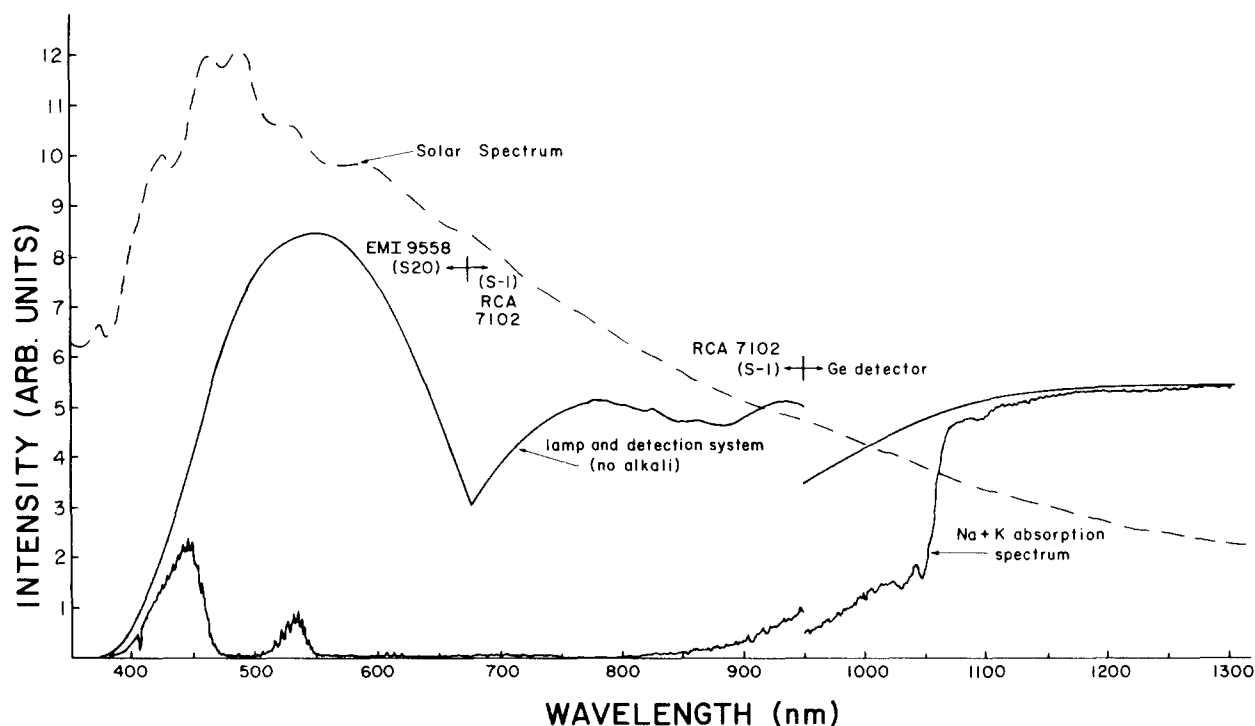
FIG. 9. Absorption spectrum obtained in the high-density jet apparatus in an $\sim$ 50–50 mixture of sodium and potassium. The total pressure was $\sim$ 147 Torr and $T \sim 728$ °C. The spectrum was obtained using the S-20 photomultiplier, the S-1 photomultiplier, and the Ge detector as indicated in the figure. Resolution for these three parts of the spectrum were 0.3, 1.1, and 0.5 nm, respectively. The dashed line represents the solar emission spectrum, for comparison (Ref. 50).

buted in Refs. 48–49 to either the K_2 triplet band, $1\ ^3\Sigma_g^+ \leftarrow 1\ ^3\Sigma_u^+$, or to absorption from a bound K_3 state. In Ref. 35 the possible identification of this band as $1\ ^3\Sigma_g^+ \leftarrow 1\ ^3\Sigma_u^+$ was eliminated, suggesting that this absorption feature should most likely be attributed to K_3. The present data is not inconsistent with this identification and the satellite feature displayed in Fig. 8 may be the first observation of a K_3 emission band. Presumably this satellite feature is buried under the NaK $1\ ^3\Pi \rightarrow 1\ ^3\Sigma^+$ band in the mixed vapor spectra. The identification of this emission feature as a K_3 band is obviously speculative at this point.

C. Absorption spectra

Alkali vapors are currently under consideration as solar absorbers for possible use in the generation of power.[36,37] A particular application being considered is in propulsion of interplanetary spacecraft.[37] A flowing gas system similar to the high-density alkali jet device[33,34] would enable the absorbing alkali to reach temperatures well in excess of those that could be withstood by the container walls since the latter are thermally isolated from the former. One attraction of alkali vapors as solar absorbers is their broad molecular absorption bands throughout the visible, near-UV, and near-IR. In particular sodium–potassium mixtures are attractive since Na_2, NaK, and K_2 would all be present with their overlapping absorption bands. Another important feature of these molecules is their lack of strong absorption and emission bands further into the infrared where the solar emission is weak. Thus power absorbed from the sun would not be

reradiated at long wavelengths as would be the case for a perfect blackbody absorber.

In view of this interest, we present in Fig. 9 a complete absorption scan between 350 and 1300 nm obtained in an $\sim$ 50–50 mixture of sodium and potassium. The total pressure was $\sim$ 147 Torr. As can be seen, at this pressure the Na–K mixture absorbs almost all incident light between 450 and 1050 nm. A solar emission spectrum is also plotted for comparison. The solar emission and alkali absorption spectra correspond well. Higher pressure vapors would be even more efficient and would probably extend the range of absorbed wavelengths further into the UV.

IV. CONCLUSIONS

In this paper we have presented new data on the near-infrared spectra of the heteronuclear alkali molecule NaK. In particular, we have presented absorption, thermal emission, and laser-induced fluorescence of the $2\ ^1\Sigma^+ \rightarrow 1\ ^1\Sigma^+$ band near its long-wavelength satellite which can be compared to spectra calculated from recently published molecular potentials and dipole moments.[19]

We also have presented observations of infrared laser-induced fluorescence at wavelengths longer than the $2\ ^1\Sigma^+ \rightarrow 1\ ^1\Sigma^+$ satellite. Through studies of the dependencies of this fluorescence on laser power and the relative Na and K atom densities, as well as by comparison to spectra calculated from recently published potentials and dipole moments, we have tentatively identified this emission as $1\ ^3\Pi \rightarrow 1\ ^3\Sigma^+$ band fluorescence from the NaK molecule. If

this identification is correct this band may be attractive as a tunable, near-IR laser candidate for several reasons. First, radiation from this band is far enough out in the infrared that no alkali absorption bands would interfere with laser operation. Second, the lower state of the band is mostly repulsive so molecules in that state dissociate rapidly preventing buildup of population which can destroy the inversion. Finally, direct pumping of specific levels of the $1\,^3\Pi$ state from the ground $1\,^1\Sigma^+$ state should be possible especially for levels near the crossing between the $1\,^3\Pi$ and $2\,^1\Sigma^+$ states. This type of pumping $\Delta S \neq 0$ transitions has recently been demonstrated in Na_2.[44-45] In heavier alkali heteronuclear molecules such as RbCs, fine structure effects are much more pronounced and therefore direct population of specific levels of the $^3\Pi$ state [which should more accurately be treated in Hund's case (c) for these heavy molecules] should be rather efficient. Unfortunately, no potential curves for these molecules exist to guide the work. An experiment designed to directly populate specific levels of the RbCs $1\,^3\Pi$ state from the ground state using a Nd:YAG laser is underway in this laboratory. It is hoped that tunable lasing may be achieved on $1\,^3\Pi \rightarrow 1\,^3\Sigma^+$ transitions. We believe this RbCs $1\,^3\Pi \rightarrow 1\,^3\Sigma^+$ band is the most likely candidate for a tunable alkali near-IR laser.

Finally, we report the observation of a satellite or shoulder feature at $\lambda \sim 1.29\,\mu m$ in the emission spectrum of high density potassium vapor excited by Kr^+ laser lines. This feature may possibly be fluorescence from the triatomic molecule K_3.

ACKNOWLEDGMENTS

[1] M. M. Hessel and C. R. Vidal, J. Chem. Phys. **70**, 4439 (1979).
[2] K. K. Verma, J. T. Bahns, A. R. Rajaei-Rizi, and W. C. Stwalley, J. Chem. Phys. **78**, 3599 (1983).
[3] S. Barratt, Proc. R. Soc. London Ser. A **105**, 221 (1924).
[4] J. M. Walter and S. Barratt, Proc. R. Soc. London Ser. A **119**, 257 (1928).
[5] F. W. Loomis and M. J. Arvin, Phys. Rev. **46**, 286 (1934).
[6] S. P. Sinha, Proc. Phys. Soc. **60**, 448 (1948).
[7] E. J. Breford and F. Engelke, Chem. Phys. Lett. **53**, 282 (1978).
[8] E. J. Breford and F. Engelke, J. Chem. Phys. **71**, 1994 (1979).
[9] D. Eisel, D. Zevgolis, and W. Demtroder, J. Chem. Phys. **71**, 2005 (1979).
[10] C. -L. Chiu and H. Chang, Chem. Phys. Lett. **73**, 167 (1980).

[11] R. F. Wormsbecher, M. M. Hessel, and F. J. Lovas, J. Chem. Phys. **74**, 6983 (1981).
[12] H. Kato and C. Noda, J. Chem. Phys. **73**, 4940 (1980).
[13] H. Kato, M. Baba, and I. Hanazaki, J. Chem. Phys. **80**, 3936 (1984).
[14] A. C. Roach, J. Mol. Spectrosc. **42**, 27 (1972).
[15] R. Janoschek and H. U. Lee, Chem. Phys. Lett. **58**, 47 (1978).
[16] W. Muller, J. Flesch, and W. Meyer, J. Chem. Phys. **80**, 3297 (1984).
[17] W. Muller and W. Meyer, J. Chem. Phys. **80**, 3311 (1984).
[18] G. H. Jeung, J. P. Daudey, and J. P. Malrieu, Chem. Phys. Lett. **94**, 300 (1983).
[19] W. J. Stevens, D. D. Konowalow, and L. B. Ratcliff, J. Chem. Phys. **80**, 1215 (1984).
[20] R. J. Bieniek and R. E. Olson, Bull. Am. Phys. Soc. **29**, 783 (1984).
[21] H. Itoh, H. Uchiki, and M. Matsuoka, Opt. Commun. **18**, 271 (1976).
[22] B. Wellegehausen, S. Shahdin, D. Friede, and H. Welling, Appl. Phys. **13**, 97 (1977).
[23] J. T. Bahns, K. K. Verma, A. R. Rajaei-Rizi, and W. C. Stwalley, Appl. Phys. Lett. **42**, 336 (1983).
[24] P. Bernage, P. Niay, and H. Bocquet, J. Mol. Spectrosc. **98**, 304 (1983).
[25] B. Wellegehausen, W. Luhs, A. Topouzkhanian, and J. d'Incan, Appl. Phys. Lett. **43**, 912 (1983).
[26] W. Luhs, M. Hube, U. Schottelius, and B. Wellegehausen, Opt. Commun. **48**, 265 (1983).
[27] V. M. Kaslin and O. F. Yakushev, Sov. J. Quantum Electron. **13**, 1575 (1983).
[28] D. D. Konowalow and P. S. Julienne, J. Chem. Phys. **72**, 5815 (1980).
[29] D. D. Konowalow, M. E. Rosenkrantz, and M. L. Olson, J. Chem. Phys. **72**, 2612 (1980).
[30] D. D. Konowalow, M. E. Rosenkrantz, and D. S. Hochhauser, J. Mol. Spectrosc. **99**, 321 (1983).
[31] D. D. Konowalow and J. L. Fish (to be published).
[32] S. Shahdin, B. Wellegehausen, and Z. G. Ma, Appl. Phys. B **29**, 195 (1982).
[33] M. Ligare, Ph.D. thesis, Columbia University, 1983 (unpublished).
[34] M. Ligare, S. Schaefer, J. Huennekens, and W. Happer, Opt. Commun. **48**, 39 (1983).
[35] J. Huennekens, S. Schaefer, M. Ligare, and W. Happer, J. Chem. Phys. **80**, 4794 (1984).
[36] A. T. Mattick, A. Hertzberg, and R. Decher, J. Energy **3**, 30 (1979).
[37] R. L. Forward, Air Force Rocket Propulsion Laboratory Report No. AFRPL TR-83-067 (1983).
[38] A. Gallagher, in *Atomic Physics 4*, edited by G. zu Putlitz, E. W. Weber, and A. Winnacker (Plenum, New York, 1975), p. 559.
[39] L. K. Lam, A. Gallagher, and M. M. Hessel, J. Chem. Phys. **66**, 3550 (1977).
[40] J. P. Woerdman and J. J. de Groot, Chem. Phys. Lett. **80**, 220 (1981).
[41] J. P. Woerdman and J. J. de Groot, in *Metal Bonding and Interactions in High Temperature Systems*, edited by J. L. Gole and W. C. Stwalley, ACS Symposium Series 179 (American Chemical Society, Washington, D. C., 1982), p. 33.
[42] C. G. Carrington and A. Gallagher, Phys. Rev. A **10**, 1464 (1974).
[43] K. M. Sando and J. C. Wormhoudt, Phys. Rev. A **7**, 1889 (1973).
[44] L. Li and R. W. Field, J. Phys. Chem. **87**, 3020 (1983).
[45] L. Li, S. F. Rice, and R. W. Field, J. Mol. Spectrosc. **105**, 344 (1984).
[46] D. D. Konowalow and J. L. Fish, Chem. Phys. **84**, 463 (1984).
[47] V. E. Chertoprud, Teplofiz. Vys. Temp. **14**, 216 (1976) [High Temp. U.S.S.R., **14**, 195 (1976)].
[48] N. D. Bhaskar, E. Zouboulis, T. McClelland, and W. Happer, Phys. Rev. Lett. **42**, 640 (1979).
[49] A. Vasilakis, Ph.D. thesis, Columbia University, 1981 (unpublished).
[50] Oriel Corporation technical information "Solar Simulation".